AIAA JOURNAL
Vol. 32, No. 4, April 1994

Dynamic-Stall and Structural-Modeling Effects on Helicopter Blade Stability with Experimental Correlation

Dinesh Barwey*
Washington University, St. Louis, Missouri 63130
and
Gopal H. Gaonkar†
Florida Atlantic University, Boca Raton, Florida 33431

The effects of blade and root-flexure elasticity and dynamic stall on the stability of hingeless rotor blades are investigated. The dynamic stall description is based on the ONERA models of lift, drag, and pitching moment. The structural analysis is based on three blade models that range from a rigid flap-lag model to two elastic flap-lag-torsion models, which differ in representing root-flexure elasticity. The predictions are correlated with the measured lag damping of an experimental isolated three-blade rotor; the correlation covers rotor operations from near-zero-thrust conditions in hover to highly stalled, high-thrust conditions in forward flight. That correlation shows sensitivity of lag-damping predictions to structural refinements in blade and root-flexure modeling. Moreover, this sensitivity increases with increasing control pitch angle and advance ratio. For high-advance-ratio and high-thrust conditions, inclusion of dynamic stall generally improves the correlation.

Nomenclature

Unless otherwise stated, the symbols below are nondimensional.

a	=	linear lift curve slope, rad^{-1}
a_d, a_m	=	damping factors in dynamic stall drag and pitching moment models
b	=	airfoil semichord, $1/R$
C_d, C_{d0}	=	airfoil sectional drag coefficient and constant profile drag coefficient
C_l, C_m	=	airfoil lift and pitching moment coefficients
C_{m0}	=	airfoil pitching moment coefficient at zero angle of attack
C_{zl}, C_{l0}	=	extrapolated linear lift coefficient and lift coefficient at zero angle of attack
c, c	=	airfoil chord, m; airfoil chord, $1/R$
E_d, E_m	=	phase shift parameters in dynamic stall drag and pitching moment models
e	=	phase shift parameter for dynamic stall lift
e_h	=	blade hinge offset for the spring model (Fig. 2), $1/R$
e_1	=	length of the hub segment in modified model (Fig. 3), $1/R$
$\mathcal{G}$	=	bending-torsion coupling parameter associated with the spring model
K_β, K_ζ	=	root spring rates in flap and lag, respectively, N-m/rad
K_ϕ	=	root spring rate in torsion, N-m/rad
k	=	b/x
L	=	length of the blade from the point of support (Table 1), m
L_x, L_y	=	local aerodynamic forces (Fig. 5)
L_0	=	apparent mass lift normal to the chord line, $(1/\rho_\infty b\Omega^2 R^3)$
l	=	length of blade from hinge to tip (equal to $1 - e_h$ for the spring model and $1 - e_1$ for the modified model)
M	=	aerodynamic pitching moment, $(1/\rho_\infty b\Omega^2 R^4 c)$
M_0	=	noncirculatory aerodynamic pitching moment per unit length, $(1/\rho_\infty b\Omega^2 R^4 c)$
R	=	rotor radius, m
$\mathcal{R}$	=	flap-lag structural coupling ratio (Fig. 1)
r_d, r_m	=	frequency parameters in dynamic stall drag and pitching moment models
r_f	=	length of the root flexure (Fig. 3), $1/R$
U	=	resultant air velocity at a blade section (Fig. 5), $1/\Omega R$
u	=	axial deflection, $1/R$
v	=	lag bending deflection, $1/R$
w	=	flap bending deflection, $1/R$
w, d	=	dynamic-stall-lift frequency and damping parameters
x	=	radial distance measured from the rotor center, $1/R$
α	=	blade airfoil section angle of attack, rad
α_s	=	shaft tilt angle, rad
Γ	=	circulation per unit length, UC_l
Γ_d	=	circulationlike drag per unit length, UC_d
Γ_m	=	circulationlike pitching moment per unit length, UC_m
δ	=	pitch-rate coefficient, rad^{-1}
δ_m	=	pitching moment parameter
$\dot{\varepsilon}$	=	airfoil rotation rate with respect to the airmass
θ_f	=	prepitch of the root flexure, rad
θ_0	=	collective pitch angle, rad
λ	=	time delay parameter
μ	=	advance ratio
ρ_∞	=	air density, kg/m^3
σ	=	negative of lead-lag mode damping exponent, 1/s
ϕ	=	elastic twist, rad
ϕ_0	=	elastic twist at the blade root in Fig. 2, rad
Ω	=	rotor angular speed, rad/s
$(\cdot)$	=	$\partial(\ )/\partial\psi$
$(\ )_s$	=	quasisteady stall quantity
$(\ )_x$, $(\ )_y$	=	x and y components
$(\ )_1$, $(\ )_2$	=	unstalled and stalled components

Received June 17, 1993; revision received Oct. 27, 1993; accepted for publication Oct. 30, 1993.

*Postdoctoral Research Associate, Department of Mechanical Engineering.
†Professor, Department of Mechanical Engineering. Associate Fellow AIAA.

Introduction

PREDICTION of helicopter blade stability is an involved process, particularly in forward flight. The structural and aerodynamic components of this process are inherently nonlinear and interdependent, and a balanced sophistication is required in modeling both components. Moreover, though major strides have been made in representing blade and root-flexure structural dynamics, much of the present understanding of aeroelastic stability is based on linear or quasisteady stall aerodynamics. Indeed, only the barest beginnings have been made in accounting for dynamic stall effects on aeroelastic stability.[1,2] The interaction between dynamic stall and structural dynamics can differ significantly from the interaction between linear aerodynamics and the same structural dynamics. Thus, an analysis is needed that can systematically isolate the influence of various modeling aspects of blade and root flexure and flowfield on blade stability. Accordingly, the present investigation focuses on isolating the influence of quasisteady stall, dynamic stall, and blade and root-flexure elasticity on blade stability in hover and in forward flight. Given the complexity of such an investigation, correlating the predictions with the test data on lag damping is a concomitant of this investigation.

In the 1980s, the Aeroflightdynamics Directorate at NASA Ames undertook two experimental investigations for the lag-mode damping data of isolated rotors in hover[3] and in hover and forward flight.[4] These data have found applications as the benchmark database for validating several aerodynamic theories ranging from linear quasisteady aerodynamics to three-dimensional unsteady aerodynamics.[1,2,5–7] The correlations with the database of highly stalled forward-flight cases (advance ratio as high as 0.55 and shaft tilt angle as high as 20 deg for collective pitch angle $\theta_0 \leq 6$ deg) are hitherto treated with rigid-blade modeling with linear and quasisteady stall aerodynamics[5,6] and with ONERA dynamic stall lift and drag models.[1] Also noteworthy is a related elastic-blade correlation[2] that includes dynamic stall and dynamic wake effects; however, it uses only a lightly loaded section of the database of Ref. 4 (0 $\leq$ advance ratio $\leq$ 0.45, shaft tilt $\leq$ 10 deg, and collective pitch angle $\theta_0 \leq 3$ deg). Thus, the section of the database with high-advance-ratio and high-thrust conditions needs to be correlated by simultaneously refining the aerodynamics and structural dynamics models.

With this background, the present investigation is noteworthy in the following respects:

1) The correlation covers a database that ranges from lightly loaded hovering conditions to highly loaded, stalled forward-flight conditions of high-advance-ratio and high-shaft-tilt combinations.[4]

2) The predictions use a spring-restrained rigid flap-lag model and two elastic blade models, which differ in the simulation of root-flexure elasticity. For each of these blade models, the predictions are based on the following three theories: refined linear theory, which accounts for large angle-of-attack and reverse-flow effects on lift and has constant drag and pitching moment; quasisteady stall theory, which includes the quasisteady stall lift, drag, and pitching-moment characteristics of the airfoil section; and complete dynamic stall theory, which includes ONERA stall dynamics models of lift, drag, and pitching moment.

Thus, in summary, the correlation covers a broad range of test data. The predictions are based on Floquet method for perturbations about a periodic orbit and thus highly stalled cases may need further research. Nevertheless, the comprehensive correlation should provide an improved understanding of the strengths and weaknesses of predicting the stability of an isolated hingeless rotor blade.

Identification of the Experimental Models

The correlation pertains to a three-blade isolated hingeless rotor[4] blade that is soft in lag and relatively stiff in torsion (with torsional frequency of at least 9/revolution). To facilitate subsequent presentation of the correlation, we provide a brief introduction to the database here. Figure 1 shows the structural details of the three-blade experimental rotor. The flexure-blade assembly consists of two distinct segments: the root segment or root flexure and the airfoil portion or blade segment. Because of the multicomponent features, the assembly shows steep gradients in the mass and stiffness distributions over a short span. On the other hand, the blade segment has essentially uniform stiffness and mass distribution right up to the blade tip. The rotor blades were untwisted and untapered. The shear center, mass center, area center, and aerodynamic center of the airfoil section were designed to be located at the quarter-chord point from the leading edge. The rotor was operated untrimmed with collective pitch θ_0 and the rotor shaft angle α_s as known control parameters for a given advance ratio. Such features of blade design and rotor operation simplify the prediction process and increase the reliability of the database.[1]

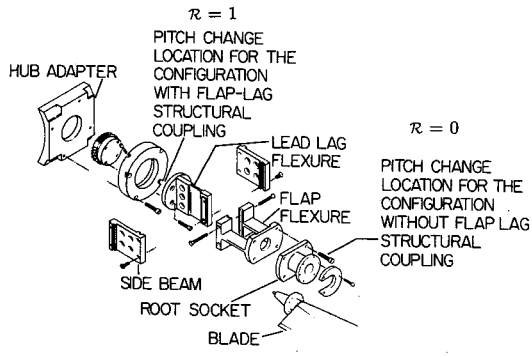

Fig. 1 Exploded view of blade and flexure assembly.[4]

Description of Analytical Models

To investigate the sensitivity of damping predictions to blade and root-flexure modeling, three generic blade models are exercised. The first one is a rigid flap-lag model with root springs, which was used earlier in Refs. 1 and 8 to correlate with the lag-damping data of Ref. 4. The other two are the elastic blade models, which are schematically presented in Figs. 2 and 3. For convenience, they are referred to as the spring model and the modified model.

Spring Model

The root-flexure elasticity is simulated by a set of three linear, massless springs located at an effective hinge offset from the rotor center. The blade is modeled as an isotropic beam with uniform mass and stiffness properties. The blade stiffness and mass properties and the flexure spring rates are based on the values reported in Ref. 4. As shown in Fig. 2, a generic material point on the elastic axis of the blade cross section undergoes axial deformation u, in-plane bending deflection v, and out-of-plane bending deflection w. The blade cross section also undergoes elastic twist ϕ and warping (not shown).

Reverting to Fig. 1, it is seen that when the pitch change takes place inboard of the root-flexure assembly, the root flexure also rotates with the blade. This rigid-body rotation of the root flexure introduces structural flap-lag coupling. When the pitch change takes place outboard of the root flexure, the principal axes of the flexure do not rotate, and hence no structural flap-lag coupling is introduced at the root. The analytical model of Fig. 2 simulates these cases by two separate pitch changes, one for root flexure, θ_f, and the other for blade, θ_0. For a finite, nonzero value of θ_f, the flap-lag spring system at the root rotates by that amount and introduces flap-lag coupling in the reference direction ($\theta_f = 0$ deg). For $\theta_f = \theta_0$ and 0 deg, the analytical model simulates, respectively, the cases of full and zero structural flap-lag cou-

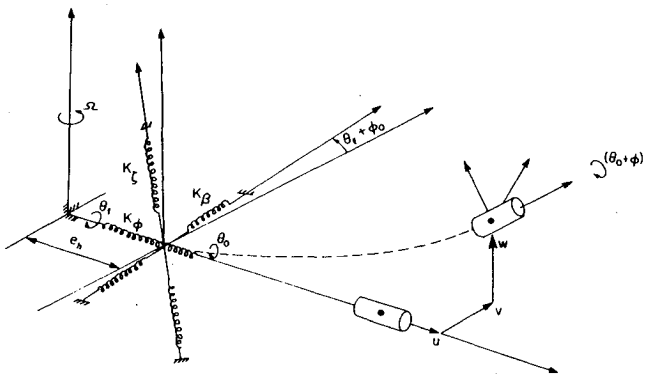

Fig. 2 Schematic of spring model.

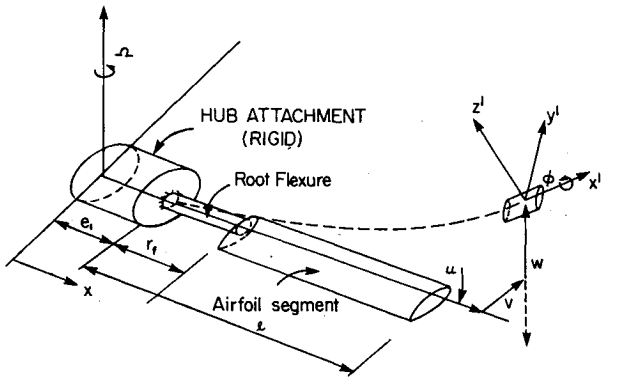

Fig. 3 Schematic of modified model.

plings ($\mathcal{R}$ = 1 and 0) of the three-blade experimental rotor shown in Fig. 1.

Figure 2 shows that the flap-lag spring system (K_β, K_ζ) also rotates by an amount that is the elastic twist that exists at the root due to finite stiffness of the root flexure. This elastic rotation of the flap-lag spring system introduces bending-torsion couplings (pitch-lag and pitch-flap) due to root-flexure elasticity. As will become clear in the sequel, these couplings affect the lag-damping predictions.

To account for a wide spectrum of design features of the root-flexure assembly, a scaling factor $\mathcal{G}$ can be applied to the bending-torsion coupling terms, which originate because of root-flexure stiffnesses with steep gradients. Although simplistic, such a factor can provide a means of monitoring the amount of the structural bending-torsion coupling due to root-flexure elasticity. Physically, $\mathcal{G}$ calibrates the amount of "elastic twist" that the flap-lag spring system undergoes due to torsional flexibility at the root. For example, $\mathcal{G}$ = 0 signifies that the flap-lag spring system does not undergo any elastic twist (in other words, $\mathcal{G}$ = 0 suppresses the bending-torsion couplings of the root flexure), whereas $\mathcal{G}$ = 1 signifies that it undergoes full elastic twist that occurs at the root (i.e., $\mathcal{G}$ = 1 includes fully the bending-torsion couplings of the root flexure). In the present work the flap-lag-torsion analysis based on the spring model is exercised with $\mathcal{G}$ = 0 and 1 to study the effects of root-flexure couplings on lag damping. It is important to mention that the factor $\mathcal{G}$ does not affect the bending-bending couplings since it is associated with the elastic torsion of the flap-lag spring set. Moreover, the cases of $\mathcal{G}$ = 0 and 1 are probably two extremes for the simulation of bending-torsion couplings of the root flexure. This is because the spring model does not incorporate the effects of distributed mass and stiffness properties in the root region. Recognizing these limitations of the spring model, we also investigate a modified model.

Modified Model

It replaces the point approximation of root-flexure elasticity of the spring model by distributing its elasticity over a finite length that is representative of the physical length of the root flexure. A schematic of this representation is shown in Fig. 3.

Except for the root-flexure simulation, the other details of this model are identical to those of the spring model. In Fig. 3, the first segment of the rotor blade (x = 0 to e_1) is modeled as infinitely rigid to simulate the highly stiff portion of the rotor hub. It is equivalent to the effective hinge offset of the spring model. The second segment, extending from $x = e_1$ to $e_1 + r_f$, simulates the distributed elasticity of the root flexure. The mass and stiffness properties in the root segment are kept uniform over its length. They are chosen so as to reasonably match the fundamental, nonrotating bending and torsion frequencies of the modified model to those of the experimental model and thus to those of the spring model. It was observed that the mass distribution in the root flexure had very little influence on the frequencies, and hence the mass per unit length in the root segment was taken equal to the corresponding value for the airfoil segment. Finally, the third segment (i.e., the airfoil segment ranging from $x = e_1 + r_f$ to 1) is again modeled as an isotropic beam with uniform stiffness and mass distributions as in the spring model. Similarly, as in the spring model, the pitch angle of the root beam, θ_f, can be set independently of the collective pitch of the airfoil portion to simulate the cases of $\mathcal{R}$ = 0 and 1 of the three-blade experimental rotor of Ref. 4. It should be mentioned that the frequencies of the modified model are sensitive to the root-flexure length r_f and the hub-segment length e_1. However, with judicious choice of these dimensions based on the experimental blade details, it is possible to reasonably match the nonrotating and rotating frequencies of the first two flap-bending, lag-bending, and torsional modes with those of the spring model.

Dynamic Stall Loading

The aerodynamic loading is based on the refined linear theory, quasisteady stall theory, and dynamic stall theory. To alleviate ambiguity of nomenclatures and to facilitate discussion of numerical results, these theories are summarized next (for details such as assumed equations of quasisteady stall characteristics, including the effects of airfoil camber, see Ref. 8).

Refined Linear Theory

Its aerodynamic lift, drag, and pitching moment components are

$$\Gamma_1 = a(U_y + b\dot{\varepsilon})\cos\alpha; \qquad \Gamma_2 = 0$$

$$\Gamma_{d_1} = UC_{d0}; \qquad \Gamma_{d_2} = 0$$

$$\Gamma_{m_1} = UC_{m_0} + \delta_m b\dot{\varepsilon}; \qquad \Gamma_{m_2} = 0$$

This theory accounts for the effects on lift of large angles of attack and reverse flow and has constant drag and pitching moment.

Quasisteady Stall Theory

It comprises the quasisteady stall lift, quasisteady stall drag, and the quasisteady stall pitching-moment characteristics of the airfoil section, as shown in Fig. 4 for the airfoil section of Ref. 4. Its components are

$$\Gamma_1 = a(U_y + b\dot{\varepsilon})\cos\alpha; \qquad \Gamma_2 = -U\Delta C_z$$

$$\Gamma_{d_1} = UC_{d0}; \qquad \Gamma_{d_2} = -U\Delta C_d$$

$$\Gamma_{m_1} = UC_{m_0} + \delta_m b\dot{\varepsilon}; \qquad \Gamma_{m_2} = -U\Delta C_m$$

where ΔC_z is the difference between the extrapolated linear lift coefficient and the quasisteady stall lift coefficient; see Fig. 4a. Similarly, ΔC_d and ΔC_m are the analogous differences

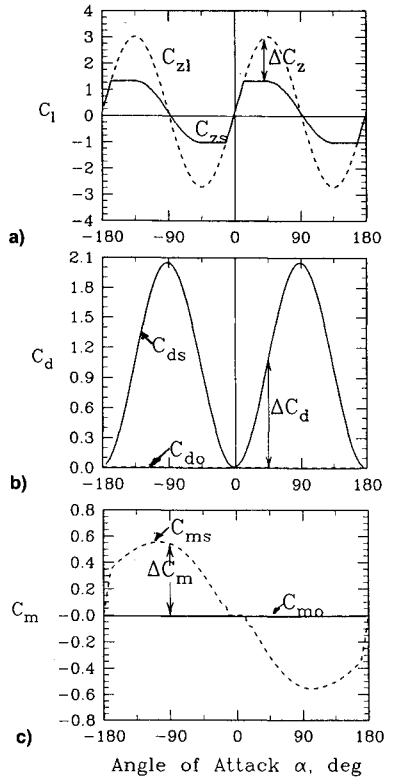

Fig. 4 Aerodynamic coefficients.

between the constant values, C_{d0} and C_{m0}, and the quasisteady stall values, C_{ds} and C_{ms}, for the drag and pitching-moment coefficients; also see Figs. 4b and 4c.

Dynamic Stall Theory[9-11]

As a complete dynamic stall theory, it comprises all three dynamic stall models of lift, drag, and pitching moment. These models are based on the ONERA description of dynamic stall unified lift, drag, and pitching moment. The lift-circulation and circulationlike drag and pitching-moment variables of dynamic stall theories are as follows:

Dynamic stall lift:

$$k\dot{\Gamma}_1 + \lambda\Gamma_1 = \lambda a(U_y + b\dot{\varepsilon})\cos\alpha + \delta b\dot{\varepsilon}$$

$$k^2\ddot{\Gamma}_2 + 2dwk\dot{\Gamma}_2 + w^2(1 + d^2)\Gamma_2 = -w^2(1 + d^2)\left[U\Delta C_z + ek(\dot{U}_x\cos\alpha + \dot{U}_y\sin\alpha)\Delta C_z + ek(\dot{U}_y\cos\alpha - \dot{U}_x\sin\alpha)\frac{\partial\Delta C_z}{\partial\alpha}\right]$$

Dynamic stall drag:

$$\Gamma_{d_1} = UC_{d0}$$

$$k^2\ddot{\Gamma}_{d_2} + a_d k\dot{\Gamma}_{d_2} + r_d^2\Gamma_{d_2} = -(r_d^2 U\Delta C_d + E_d k\dot{U}_y)$$

Dynamic stall pitching moment:

$$\Gamma_{m_1} = UC_{m0} + \delta_m b\dot{\varepsilon}$$

$$k^2\ddot{\Gamma}_{m_2} + a_m k\dot{\Gamma}_{m_2} + r_m^2\Gamma_{m_2} = -(r_m^2 U\Delta C_m + E_m k\dot{U}_y)$$

The various coefficients of the dynamic stall models (e.g., λ, δ, w, a_d, E_d, r_m, E_m, etc.) in the previous equations are determined on the basis of wind-tunnel experiments for a given airfoil.[8,11]

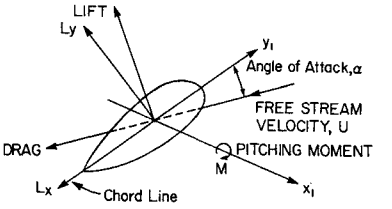

Fig. 5 Schematic of blade aerodynamics.

The aerodynamic forces and pitching moment in terms of the previous aerodynamic variables on a local airfoil section are (see Fig. 5)

$$L_y = U_x(\Gamma_1 + \Gamma_2) + U_y(\Gamma_{d_1} + \Gamma_{d_2}) + L_0$$

$$L_x = -U_y(\Gamma_1 + \Gamma_2) + U_x(\Gamma_{d_1} + \Gamma_{d_2})$$

$$M = 2b[U(\Gamma_{m_1} + \Gamma_{m_2})] + M_0$$

where L_x, L_y, and M represent, respectively, the drag force acting along the chord line, the nondimensional lift force acting normal to the chord line at the aerodynamic center, and the pitching moment about the aerodynamic center of the airfoil; U_x and U_y are the local velocity components of the resultant air velocity U in the local blade coordinate system; that is, $U_x = U\cos\alpha$ and $U_y = U\sin\alpha$; and L_0 and M_0 represent the noncirculatory lift and pitching moment, respectively, that are functions of the airfoil rotation rate with respect to the airmass $\dot{\varepsilon}$.

As seen earlier, the inclusion of dynamic stall into rotor blade analysis involves additional differential equations and introduces the so-called aerodynamic states in the formulation. Specifically, in addition to nonlinear equations of motion, now there are three second-order differential equations and one first-order differential equation for every spanwise station.

Analysis

A brief account of the formulation and solution is included; for details see Ref. 8.

The nonlinear elastodynamic equations of blade motions are derived using Hamilton's principle. The equations are based on a second-order ordering scheme. The formulation requires development of variational strain energy, potential energy of root springs, kinetic energy, and virtual work of nonconservative aerodynamic loading. The resulting system consists of three second-order partial differential equations (for flap, lag, and torsional motions) with periodic coefficients in forward-flight conditions. The spatial dependency of the equations is eliminated by a modified Galerkin's technique to yield a set of ordinary differential equations in nondimensional time.

To apply Galerkin's method, a set of orthogonal mode shapes for flap bending, lag bending, and torsion is developed that account for the root flexure and blade elasticity. They are based on the equations of an uncoupled, nonrotating, freely vibrating beam. For the spring model of Fig. 2, spring restrained at one end and free at the other, it is a straightforward exercise. For the modified model of Fig. 3, symbolic processor REDUCE is used to derive the bending modes of a stepped beam with one end fixed and the other free ($x = e_1$ and 1, respectively, in Fig. 3). To account for the discontinuity in the stiffness distributions at the junction $x = e_1 + r_f$, the bending displacements, bending slopes, bending moments, and shear forces are made continuous; similarly, the twist and torsional moments are made continuous at the junction for the torsional mode shapes. The predictions use two modes each for flap bending, lag bending, and torsion and zero prepitch of the root flexure, i.e., $\theta_f = 0$ deg.

In the Floquet analysis, the time-dependent second-order differential equations are analytically perturbed about a pe-

riodic orbit to obtain linearized differential equations. A consistent perturbation scheme requires that the dynamic stall equations also be perturbed and linearized about the same periodic orbit along with all of the coefficients and quantities of the dynamic stall models of lift, drag, and pitching moment. A numerical integration scheme that uses five elements of equal length along the blade span is employed for evaluation of the aerodynamic contributions. The periodic orbit is established by a periodic shooting strategy. Damping levels are determined from Floquet eigenanalysis.

Results

The predictions and correlations with the test data of the experimental rotor[4] are voluminous. Therefore, an important section of that correlation is presented with emphasis on high-thrust, forward-flight regimes. Accordingly, in Figs. 6–10, shaft tilt as high as 16 deg is selected and the flap-lag coupling ratio $\mathcal{R} = 0$. Moreover, the advance ratio μ varies from hover to very high-speed conditions with μ as high as 0.55, and two values of collective pitch angle are selected for each sweep of advance ratio. Reiterating, in Figs. 6–10, $\mathcal{R} = 0$, $\alpha_s = 16$ deg, $0 \leq \mu \leq 0.55$; part "a" of each figure refers to $\theta_0 = 0$ deg; part "b" refers to $\theta_0 = 3$ deg, and the fundamental lag-mode damping levels are plotted vs advance ratio.

In addition to the correlations based on the spring model (Fig. 2) and the modified model (Fig. 3), Figs. 6–10 include predictions based on simpler structural models as well. This helps identify the effects of various modeling ingredients that participate in the correlation, e.g., blade bending, root-flexure bending, blade torsion, root-flexure torsion, etc. To facilitate subsequent discussion of results without any ambiguity of terminology, a brief account of five structural models identified in Figs. 6–10 follows.

1) Rigid flap-lag analysis: This analysis and the results are discussed in detail in Refs. 1 and 8. Results presented in those references are used here for a comparative assessment of rigid-blade vis-a-vis elastic-blade predictions.

2) Flap-lag analysis: It is obtained by suppressing the torsional degrees of freedom from the elastic flap-lag-torsion formulation of the spring model (Fig. 2). It represents an improvement over the rigid flap-lag analysis by incorporating elastic-bending effects. The root-flexure elasticity is simulated by a set of flap-lag springs.

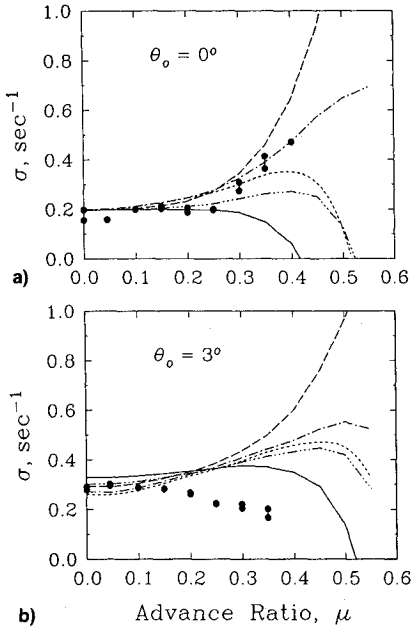

Fig. 6 Structural modeling effects on lag-damping correlation in forward flight with refined linear theory, $\alpha_s = 16$ deg (•, test data at 1000 rpm; ---, rigid flap-lag analysis; — · —, flap-lag analysis; — — —, flap-lag-torsion analysis with $\mathcal{G} = 0$; ———, flap-lag-torsion analysis with $\mathcal{G} = 1$; — · · · —, modified flap-lag-torsion analysis).

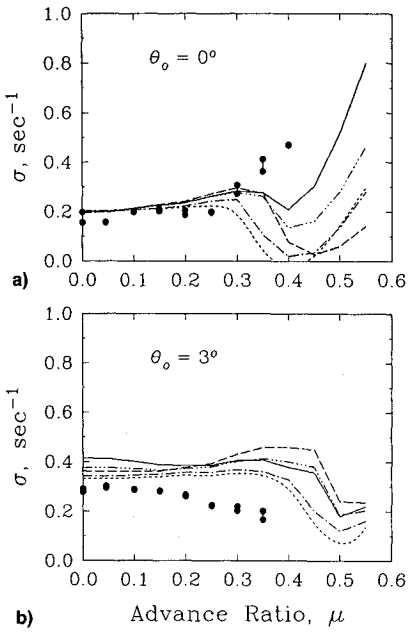

Fig. 7 Structural modeling effects on lag-damping correlation in forward flight with quasisteady stall theory, $\alpha_s = 16$ deg (•, test data at 1000 rpm; ---, rigid flap-lag analysis; — · —, flap-lag analysis; — — —, flap-lag-torsion analysis with $\mathcal{G} = 0$; ———, flap-lag-torsion analysis with $\mathcal{G} = 1$; — · · · —, modified flap-lag-torsion analysis).

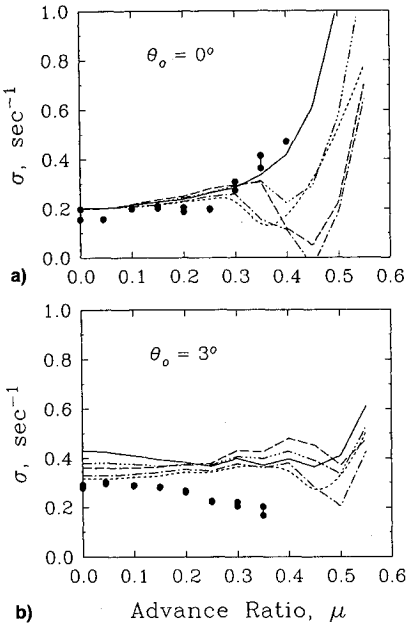

Fig. 8 Structural modeling effects on lag-damping correlation in forward flight with dynamic stall theory, $\alpha_s = 16$ deg (•, test data at 1000 rpm; ---, rigid flap-lag analysis; — · —, flap-lag analysis; — — —, flap-lag-torsion analysis with $\mathcal{G} = 0$; ———, flap-lag-torsion analysis with $\mathcal{G} = 1$; — · · · —, modified flap-lag-torsion analysis).

3) Flap-lag-torsion analysis ($\mathcal{G} = 0$): It represents an improvement over the elastic flap-lag analysis by incorporating the elastic torsional degrees of freedom. However, the bending-torsion structural couplings (pitch-lag and pitch-flap couplings) from root-flexure elasticity are ignored by assigning the value zero to the scaling parameter $\mathcal{G}$.

4) Flap-lag-torsion analysis ($\mathcal{G} = 1$): It fully accounts for the bending-torsion couplings originating from the root-flexure elasticity. Comparisons with the previous analysis with $\mathcal{G} = 0$ isolate the effects of bending-torsion couplings from root-flexure elasticity.

5) Modified flap-lag-torsion analysis: It is based on the modified elastic blade formulation in which the root flexure

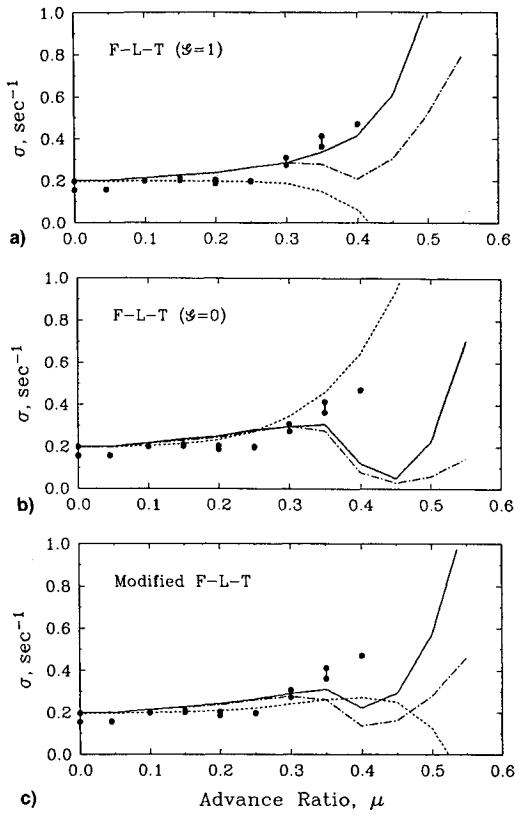

Fig. 9 Aerodynamic modeling effects on lag-damping correlation in forward flight, θ_0 = 0 deg and α_s = 16 deg (•, test data at 1000 rpm; ---, refined linear theory; — · —, quasisteady stall theory; ———, dynamic stall theory).

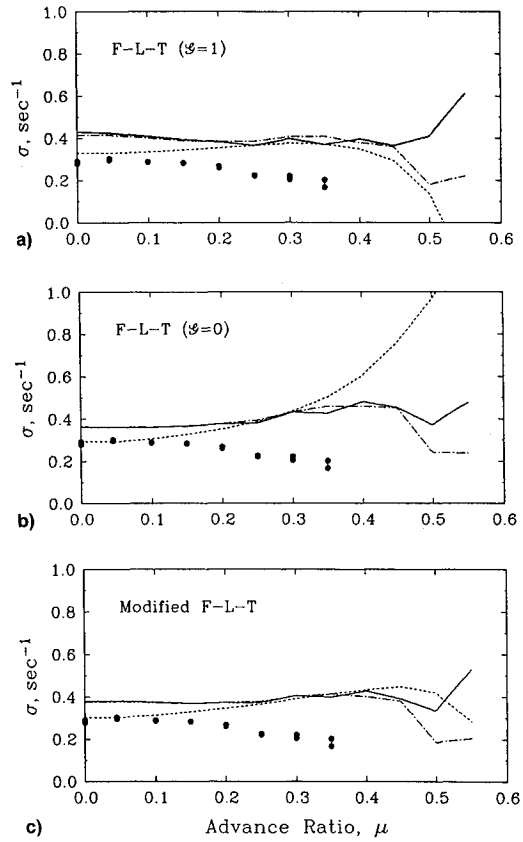

Fig. 10 Aerodynamic modeling effects on lag-damping correlation in forward flight, θ_0 = 3 deg and α_s = 16 deg (•, test data at 1000 rpm; ---, refined linear theory; — · —, quasisteady stall theory; ———, dynamic stall theory).

is modeled as a short uniform beam (Fig. 3). The purpose is to study the effect of distributed elasticity of root flexure as compared with its point approximation; compare Fig. 3 with Fig. 2. It was observed that the flap-lag analysis based on the modified model (Fig. 3) is almost identical to that based on the spring model (Fig. 2) for all three aerodynamic models, and hence it is not separately exercised.

Refined Linear Theory

Figure 6 shows the lag-damping correlation based on the refined linear theory. In Fig. 6a for θ_0 = 0 deg, the test data show an almost constant damping level till an advance ratio of about 0.25 and then a sharp increase in damping with increasing advance ratio. For low advance ratios ($\mu \leq 0.25$) with low thrust levels, the correlation between two flap-lag analyses and test data is adequate. The rigid flap-lag analysis shows a sharp decrease in damping for $\mu > 0.40$, which is in contrast to the trend of the data. On the other hand, the flap-lag analysis shows steadily increasing damping with advance ratio, in general agreement with the data. At advance ratio $\mu > 0.35$, the deviation of the rigid flap-lag analysis from the elastic flap-lag analysis in Fig. 6a is due to flap and lag bending effects. Though not shown, it was observed that the first flap-bending, the first lag-bending, and the second flap-bending effects are primarily responsible for this deviation. The dimensionless modal frequencies in Table 1 support these observations; the first and second flap modes with frequencies of 1.105 and 3.41, respectively, are the closest to the lag natural frequency of 0.604. All other bending mode frequencies are well separated from the fundamental lag frequency. Concerning torsion, though the second mode ceases to be an issue (0.604 vs 27.94), the sensitivity of lag damping to bending-torsion couplings becomes an issue, as discussed next.

Figure 6a includes predictions from the modified flap-lag-torsion analysis in which, as mentioned earlier, the root-flexure elasticity is simulated by a short beam with uniform stiffness distribution. It also includes predictions from the spring model, that is, flap-lag-torsion analyses with $\mathcal{G}$ = 0 and 1. At low advance ratios ($\mu < 0.25$), the predictions of all three flap-lag-torsion analyses are fairly close because of relatively low-thrust flight conditions. However, at higher advance ratios the three analyses deviate quantitatively and qualitatively. For example, with increasing advance ratio, the flap-lag-torsion analysis of the spring model with $\mathcal{G}$ = 0 shows increasing damping, whereas with $\mathcal{G}$ = 1 it shows decreasing damping. Interestingly, the modified flap-lag-torsion analysis exhibits a sort of average of the other two analyses (i.e., $\mathcal{G}$ = 0 and 1) of the spring model. These deviations, among three flap-lag-torsion analyses, are because of the differences in simulating bending-torsion couplings of the root flexure. They illustrate the importance of root-flexure modeling on lag-damping predictions in forward flight, especially under high-thrust conditions.

A comparison of the flap-lag analysis with three flap-lag-torsion analyses in Fig. 6a shows that the torsional degree of freedom has little impact at low-thrust conditions ($\mu \leq 0.25$). Its influence, however, builds as the advance ratio increases. Additional results (not shown) reveal that this buildup is primarily due to pitch-flap and pitch-lag couplings of the root flexure and blade. Overall, the flap-lag analysis and the flap-lag-torsion analysis with $\mathcal{G}$ = 0 provide excellent correlation.

Table 1 Rotating frequencies for the experimental rotor of Ref. 4[a]

	Dimensionless, 1/Ω		
Mode	Flap	Lag	Torsion
First	1.105	0.604	9.166
Second	3.41	10.66	27.94
Third	7.96	33.67	45.82

[a]Uncoupled at $\theta_f = \theta_0 = 0$ deg from the spring model.

By comparison, the other three analyses do not predict the trend of the data of increasing damping with increasing advance ratio for the entire data range from hover to $\mu = 0.4$. However, varying degrees of correlation from different models perhaps indicate that correlation with a wider database (e.g., with the data for $\theta_0 = 3$ deg) is required before we pass judgment on the relative merits of these structural models. This is done in Fig. 6b.

Figure 6b shows slowly decreasing damping data with increasing advance ratio, which is in contrast to the trend of the data in Fig. 6a. However, the predictions from the five structural analyses in Fig. 6b for $\theta_0 = 3$ deg are similar to those in Fig. 6a for $\theta_0 = 0$ deg. Thus, the contrast in the trend of the data for the two collective pitch angles merits further interpretation of predictions from different structural analyses. For $\theta_0 = 3$ deg, the two flap-lag analyses (rigid and elastic) are in contrast to the data even at low advance ratios ($\mu \leq 0.25$) as they both show increasing damping with increasing advance ratio. At very high advance ratios, say $\mu > 0.4$, the rigid-blade analysis shows a reduction in damping, but that reduction is so delayed that it becomes almost qualitatively inaccurate. The predictions from the flap-lag-torsion analysis with $\mathcal{G} = 0$ again show sharply increasing damping with advance ratio throughout, which renders it qualitatively inaccurate as well. Though not shown, it was found that the neglect of bending-torsion couplings of the blade (conventional blade pitch-lag and pitch-flap couplings) account for the difference between the elastic flap-lag and the elastic flap-lag-torsion ($\mathcal{G} = 0$) analyses at low advance ratios ($\mu \leq 0.25$). The inclusion of bending-torsion couplings from root flexure ($\mathcal{G} = 1$) brings in qualitative changes in the predictions of flap-lag-torsion analysis without these couplings ($\mathcal{G} = 0$). At low advance ratios ($\mu \leq 0.25$), these root-flexure couplings result in slightly higher damping, whereas at high advance ratios the role is reversed, i.e., these couplings tend to reduce the damping appreciably in comparison to the analysis with $\mathcal{G} = 0$. At high advance ratios, this reversal degrades correlation for $\theta_0 = 0$ deg (Fig. 6a) and improves correlation for $\theta_0 = 3$ deg (Fig. 6b). Moreover, in Fig. 6b, replacement of the point approximation of root-flexure elasticity in the flap-lag-torsion analyses ($\mathcal{G} = 0$ and 1) of the spring model by root-flexure element as incorporated in the modified flap-lag-torsion analysis brings in further quantitative changes in the predictions and correlation. At low advance ratios, relative to the predictions with this replacement, the flap-lag-torsion analysis with $\mathcal{G} = 1$ slightly overpredicts lag damping, and the analysis with $\mathcal{G} = 0$ slightly underpredicts. At higher advance ratios the reverse is the case, but the under- and overpredictions are far more pronounced. It is instructive to mention that with $\mathcal{G} = 0.63$ the flap-lag-torsion analysis of the spring model provides predictions almost identical to the ones from the modified flap-lag-torsion analysis for $\theta_0 = 0$ and 3 deg for the entire data range. This value of $\mathcal{G}$ gives a measure of equivalence between the spring model of Fig. 2 and the modified model of Fig. 3. It basically represents a fraction of the actual elastic twist of the root that the flap-lag spring system should undergo to yield comparable bending-torsion couplings of the modified flap-lag-torsion model. Overall, the predictions are unsatisfactory because each provides reasonable correlation for one case and poor correlation for the other. For example, the flap-lag-torsion analysis with $\mathcal{G} = 1$ is reasonable at $\theta_0 = 3$ deg but qualitatively inaccurate for $\theta_0 = 0$ deg.

Quasisteady Stall Theory

The preceding correlation is further pursued by replacing the refined linear theory by the quasisteady stall theory; the same five structural analyses of Fig. 6 are used. In Fig. 7a for $\theta_0 = 0$ deg, the two flap-lag analyses show good correlation with the data for low-thrust conditions at low advance ratios ($\mu \leq 0.25$). But for high advance ratios corresponding to high-thrust conditions,[1] they show considerable divergence from the data. Inclusion of elastic torsion (as represented by flap-lag-torsion analysis with $\mathcal{G} = 0$) into elastic flap-lag analysis yields some quantitative changes that tend to somewhat improve the correlation, particularly for $\mu > 0.3$. These changes indicate the blade bending-torsion coupling effects. Inclusion of root-flexure bending-torsion couplings ($\mathcal{G} = 1$) are seen to provide almost qualitative changes in the predictions when compared with the flap-lag-torsion analysis with $\mathcal{G} = 0$. For example, the elastic flap-lag-torsion analysis ($\mathcal{G} = 0$) shows severe loss in damping at high advance ratio; however, with $\mathcal{G} = 1$, that loss is much reduced. Similar to the refined linear theory prediction in Fig. 6a, the modified flap-lag-torsion analysis provides predictions in between the flap-lag-torsion analyses with $\mathcal{G} = 0$ and 1; indeed, the flap-lag-torsion analysis with $\mathcal{G} = 0.63$ is found to be virtually identical to the modified flap-lag-torsion analysis throughout. The quantitative difference between the three elastic flap-lag-torsion analyses again illustrates the sensitivity of lag damping predictions to modeling the root flexure under stalled forward-flight conditions.

The quasisteady stall theory for $\theta_0 = 3$ deg is illustrated in Fig. 7b. The rigid flap-lag and elastic flap-lag analyses provide comparable predictions and yield reasonable correlations within the data range, $0 \leq \mu \leq 0.35$. For very high advance ratios ($\mu > 0.4$), both analyses show loss in lag damping, which is beyond the data range. On the other hand, in comparison with the flap-lag-torsion analysis with $\mathcal{G} = 0$, the analysis with $\mathcal{G} = 1$ at low advance ratios shows a trend of decreasing damping with increasing advance ratio. The tradeoff for this qualitative improvement is a slight quantitative degradation in correlation, particularly at low advance ratios. The modified flap-lag-torsion analysis again yields predictions that are in between the predictions of flap-lag-torsion analyses with $\mathcal{G} = 0$ and 1. At hovering and low-advance-ratio conditions, the modified flap-lag-torsion analysis in Fig. 7b shows that the flap-lag-torsion analysis with $\mathcal{G} = 1$ has perhaps overestimated the effects of bending-torsion couplings of the root flexure. This overestimation is evidenced by the fact that the flap-lag-torsion analysis with $\mathcal{G} = 0.63$ (Fig. 2) simulates throughout the modified flap-lag-torsion analysis (Fig. 3), as was the case in Fig. 6b based on linear theory. Overall, Fig. 7 shows that the modified flap-lag-torsion analysis and flap-lag-torsion analysis with $\mathcal{G} = 1$ provide, at best, fair correlation with quasisteady stall theory for both cases of database with $\theta_0 = 0$ and 3 deg.

Dynamic Stall Theory

Figure 8 is based on the dynamic stall theory. The predictions in Fig. 8a for $\theta_0 = 0$ deg and in Fig. 8b for $\theta_0 = 3$ deg are somewhat similar to their respective counterparts in Figs. 7a and 7b based on the quasisteady stall theory.

Figure 8a shows that at low advance ratios ($\mu \leq 0.25$) the differences among the five structural analyses are marginal. Also, it shows negligible effect of torsion at low-thrust and low-advance-ratio conditions. However, at high advance ratios ($\mu > 0.25$), the flap-lag-torsion analysis with $\mathcal{G} = 1$ shows significant deviation from the rigid flap-lag analysis. This difference is partly due to blade bending (as shown by the difference between the elastic flap-lag and the rigid flap-lag analyses) and partly due to blade torsion (as shown by the difference between the elastic flap-lag analysis and the flap-lag torsion analysis with $\mathcal{G} = 0$) and root torsion (as shown by the difference between the two flap-lag-torsion analyses from the spring model in Fig. 2 with $\mathcal{G} = 0$ and 1). Similarly, the deviation of the modified flap-lag-torsion analysis from the two flap-lag-torsion analyses ($\mathcal{G} = 0$ and 1) signifies the effects of the point approximation of root flexure vis-a-vis the short-beam approximation. It is remarkable that both the modified flap-lag-torsion analysis and the rigid flap-lag analysis predict similar trends of lag damping. Overall, the flap-lag-torsion analysis with $\mathcal{G} = 1$ gives very good correlation.

The correlation in Fig. 8b for $\theta_0 = 3$ deg shows that all three elastic flap-lag-torsion analyses overpredict damping as compared with the elastic flap-lag and rigid flap-lag analyses for the entire data range. At low advance ratios much of this overprediction was found to be associated with the quasisteady torsional effects that introduce pitch-lag and pitch-flap couplings of the root flexure. At high advance ratios, the reasons for this overprediction are difficult to isolate, and research is continuing. At low advance ratios elastic flap-lag analysis is fairly close to the rigid-blade analysis. For the entire data range ($0 \leq \mu \leq 0.35$), although the rigid-blade analysis is quantitatively closer to the data, it fails to predict the trend of the data of decreasing damping with increasing advance ratio. That trend is predicted by the flap-lag-torsion analysis with $\mathcal{G} = 1$ in spite of quantitative deviation.

Comparison of Aerodynamic Theories

It is of interest to see the effects of aerodynamic refinements for a particular structural model. For this purpose, Figs. 9 and 10 show the comparison of the three aerodynamic theories—refined linear, quasisteady stall, and dynamic stall—for $\theta_0 = 0$ and 3 deg. These figures contain predictions that are extracted from Figs. 6–8 corresponding to the two flap-lag-torsion analyses of the spring model (with and without bending-torsion couplings of the root flexure, i.e., $\mathcal{G} = 1$ and 0, respectively) and the modified flap-lag-torsion analysis.

For $\theta_0 = 0$ deg, Fig. 9a from the flap-lag-torsion analysis with $\mathcal{G} = 1$ shows that all three aerodynamic theories are close to each other at low advance ratios due to low-thrust conditions. For $\mu > 0.25$, with increasing thrust, the two stall theories start to deviate from the refined linear theory, which shows steadily decreasing damping in contrast to the trend of the data. But the two stall theories show an overall increasing damping trend in accordance with the data. These two stall theories are identical up to an advance ratio of 0.30, and then dynamic stall comes into play, which results in higher damping from the dynamic stall theory as compared with quasisteady stall theory. The quasisteady stall theory shows a loss in damping at $\mu = 0.4$ and then a sharp gain in damping. This loss is absent for the dynamic stall theory, nor is it supported by the data. When the bending-torsion couplings of the root flexure are eliminated by setting $\mathcal{G} = 0$, the resulting trends of damping from the three aerodynamic theories are shown in Fig. 9b. This elimination has significant impact on all three theories at $\theta_0 = 0$ deg. Each of the aerodynamic theories in Fig. 9b with $\mathcal{G} = 0$ changes the general direction as compared with those in Fig. 9a with $\mathcal{G} = 1$. For example, the refined linear theory in Fig. 9b shows increasing damping trend in contrast to its trend of decreasing damping in 9a. At very high advance ratios, as shown in Fig. 9b for $\mu > 0.45$, the two stall theories begin to show some recovery from the loss in damping, but the recovery is well delayed with respect to advance ratio.

Figure 9c shows the comparison of the aerodynamic theories based on the modified flap-lag-torsion analysis. As discussed earlier, the aerodynamic theories in Fig. 9c represent some average of their respective counterparts in Figs. 9a and 9b. Noticeable in Fig. 9c is a lack of excessive quantitative deviation of the refined linear theory from the two stall theories within the data range, $\mu \leq 0.4$.

Similar effects of aerodynamic refinements for a collective pitch angle of $\theta_0 = 3$ deg are illustrated in Figs. 10a and 10b for the flap-lag-torsion analyses with $\mathcal{G} = 1$ and 0, respectively, and in Fig. 10c for the modified flap-lag-torsion analysis. As seen in Fig. 10a, the two stall theories show a slightly decreasing damping trend for $\mu \leq 0.25$, and then the damping somewhat levels off right up to the end of the data range at $\mu = 0.35$. The refined linear theory in Fig. 10a shows a small gain in damping for the entire data range, ($0 \leq \mu \leq 0.35$) and then shows a rapid loss in damping. The exclusion of bending-torsion couplings of the root flexure, as embodied in Fig. 10b, has the most significant impact on the refined linear theory, which shows sharp increase in damping with advance ratio that is opposite to the trend of the data. The two stall theories in Fig. 10b also differ from their counterparts in Fig. 10a quantitatively by showing a net increase in damping for the entire data range. However, in the modified flap-lag-torsion analysis of Fig. 10c this increase is almost absent. The two stall theories in Fig. 10c show that damping slightly decreases for $0.0 \leq \mu \leq 0.25$ in accordance with the data, which shows consistently decreasing damping throughout. The refined linear theory in Fig. 10c shows consistently increasing damping, and as such it is qualitatively inaccurate. It is worth mentioning that the differences between the two stall theories and the refined linear theory in Figs. 10a, 10b, and 10c, at low advance ratios, are caused by nonlinear drag effects owing to the low-Reynolds-number condition of the test data.

Overall, the dynamic stall theory with modified flap-lag-torsion and with flap-lag-torsion analysis that fully accounts for bending-torsion coupling of the root flexure ($\mathcal{G} = 1$) provides good correlation for $\theta_0 = 0$ deg and, at best, fair correlation for $\theta_0 = 3$ deg.

Conclusions

The correlation with the lag-damping database of Ref. 4 leads to the following findings:

1) The bending-torsion couplings due to root-flexure elasticity have significant impact on the stability of the three-blade experimental rotor of Ref. 4.

2) The predictions show sensitivity to structural refinements, and this sensitivity increases with increasing pitch setting and increasing advance ratio.

3) Despite the high blade torsional frequency, the torsional degree of freedom has significant impact on the stability of lag motion. At low advance ratios, it manifests mainly through quasisteady bending-torsion (pitch-lag and pitch-flap) couplings of the root flexure and blade. With increasing advance ratios, because of increasing flowfield complexity, the interaction of quasisteady and dynamic torsion becomes increasingly difficult to interpret.

4) Overall, the dynamic stall aerodynamic representation and the structural representation based on the modified flap-lag-torsion model (Fig. 3) as well as on the flap-lag-torsion model with $\mathcal{G} = 1$ (Fig. 2) give good correlation for $\theta_0 = 0$ deg and, at best, fair correlation for $\theta_0 = 3$ deg.

Acknowledgments

This work was sponsored by the Army Research Office under Grant DAAL03-91-G-0007 and the Army Aeroflightdynamics Directorate at NASA Ames Research Center under Grant NAG 2-797. The authors are grateful to J. Nagabhushanam of Indian Institute of Science, Bangalore, India, to David Peters of Washington University, St. Louis, and to Robert Ormiston of the Army Aeroflightdynamics Directorate at NASA Ames Research Center for their suggestions. The authors wish to acknowledge the efforts of Srinivas Chunduru in code execution and curve plotting.

References

[1]Barwey, D., Gaonkar, G. H., and Ormiston, R. A., "Investigation of Dynamic Stall Effects on Isolated Rotor Flap-Lag Stability with Experimental Correlation," *Journal of the American Helicopter Society*, Vol. 36, No. 4, 1991, pp. 12–24.

[2]Torok, M. S., and Chopra, I., "Hingeless Rotor Aeroelastic Stability Analysis with Refined Aerodynamic Modeling," *Journal of the American Helicopter Society*, Vol. 36, No. 4, 1991, pp. 48–56.

[3]Sharpe, D. L., "An Experimental Investigation of the Flap-Lag-Torsion Aeroelastic Stability of a Small Scale Hingeless Helicopter Rotor in Hover," NASA TP 2546, Aviation Systems Command TR 85-A-9, Jan. 1986.

[4]McNulty, M. J., "Flap-Lag Stability Data for a Small Scale Isolated Hingeless Rotor in Forward Flight," NASA TM 102189, April 1989.

[5]Nagabhushanam, J., Gaonkar, G. H., and McNulty, M. J., "An

Experimental and Analytical Investigation of Stall Effects on Flap-Lag Stability in Forward Flight," Thirteenth European Rotorcraft Forum Proceedings, Paper 6-2, Arles, France, Sept. 1987.

[6]Gaonkar, G. H., McNulty, M. J., and Nagabhushanam, J., "An Experimental and Analytical Investigation of Isolated Rotor Flap-Lag Stability in Forward Flight," *Journal of the American Helicopter Society*, Vol. 35, No. 2, 1990, pp. 25–34.

[7]Kwon, O. J., Hodges, D. H., and Sankar, L. N., "Stability of Hingeless Rotors in Hover Using Three-Dimensional Unsteady Aerodynamics," *Journal of the American Helicopter Society*, Vol. 38, No. 2, 1991, pp. 21–31.

[8]Barwey, D., "Dynamic Staff Effects on Hingeless Rotor Stability with Experimental Correlation," Ph.D. Dissertation, College of Engineering, Florida Atlantic Univ., Boca Raton, FL, Jan. 1992.

[9]Peters, D. A., "Toward a Unified Lift Model for Use in Rotor Blade Stability Analysis," *Journal of the American Helicopter Society*, Vol. 30, No. 3, 1985, pp. 32–42.

[10]Petot, D., and Dat, R., "Unsteady Aerodynamic Forces on an Airfoil Performing Oscillations with Unsteady Stall," *Proceedings of the Second Technical Workshop on Dynamics and Aeroelastic Stability Modeling of Rotorcraft Systems*, Army Research Office and Florida Atlantic Univ., Boca Raton, FL, Nov. 1987.

[11]Petot, D., "Differential Equation Modeling of Dynamic Stall," ONERA TN 5, 1989.